*Proceedings of the 11th Brazilian Congress of Thermal Sciences and Engineering -- ENCIT 2006*
*Braz. Soc. of Mechanical Sciences and Engineering -- ABCM, Curitiba, Brazil, Dec. 5-8, 2006*

**Paper CIT06-0466**

# EFFECT OF DIE LIP CONFIGURATION ON THE OPERATING WINDOW OF SLOT COATING PROCESS

**Danmer Maza Quinones**
Department of Mechanical Engineering
Pontifical Catholic University of Rio de Janeiro – PUC-Rio
Rua Marquês de São Vicente 225, Gávea, Rio de Janeiro, Brasil
danmerm@mec.puc-rio.br

**Márcio da Silveira Carvalho**
Department of Mechanical Engineering
Pontifical Catholic University of Rio de Janeiro – PUC-Rio
Rua Marquês de São Vicente 225, Gávea, Rio de Janeiro, Brasil
msc@mec.puc-rio.br

*Abstract.* Slot coating is a common method in the manufacture of a wide variety of products. The thickness of the coated liquid layer is set by the flow rate fed to the coating die and the speed of the substrate. The competition among viscous, capillary and pressure forces, and in some cases inertial forces, sets the range of operating parameters in which the viscous free surface flow of the liquid can be two-dimensional and steady. The region in the operating parameters of a coating process where the delivered liquid layer is uniform is referred to as coating window. The geometric configuration of the die has a strong effect on the various forces acting near the free surface. There are several die configurations disclosed in the patent literature claiming to be the optimal one. In this work, the theoretical analysis of the flow in a slot coating bead is developed. The conservation equations are solved with the Galerkin/FEM. The Coating windows are determined theoretically by searching the conditions at which the upstream or the downstream free surface invades the coating bead and the flow becomes unstable. The results show the effect of different geometric parameters on the limits of operability of the process.

*Keywords: slot coating, free surface flow, Finite Element Method.*

## 1. Introduction

Slot coating is used in the manufacturing process of adhesive and magnetic tapes, specialty papers, imaging films, and many other products. In this process, the coating liquid is pumped to a coating die in which an elongated chamber distributes it across the width of a narrow slot through which the flow rate per unit width at the slot exit is made uniform as shown in Fig.1. Exiting the slot, the liquid fills (wholly or partially) the gap between the adjacent die lips and the substrate translating rapidly past them. The liquid in the gap bounded upstream and downstream by gas-liquid interfaces, or menisci, forms the coating bead. The competition among viscous, capillary, inertial and pressure forces, sets the range of operating parameters in which the viscous free surface flow of the liquid can be two-dimensional and steady (gravitational effects are neglected because the length scale of a coating bead is so small). It is clear that physics sets the operating parameters at which this two-dimensional free surface flow exists. In order to sustain the coating bead at higher speeds, vacuum is usually applied on the back of the upstream meniscus (Beguin, 1954). This method belongs to a class of coating methods known as *pre-metered coating*: the thickness of the coated liquid layer is set by the prescribed flow rate fed into the coating die and it is independent of the process variables, making this class of method ideal for high precision coating. However, the liquid flow in the application region (coating bead), and therefore the quality of the coated film, is strongly affected by the substrate speed, the viscosity and the configuration of the die lips immediately upstream and downstream of the slot exit.

The region of acceptable coating quality in the space of operating parameters of a coating process is usually referred to as the coating window. Knowledge of coating windows of different coating methods is needed to predict whether a particular method can be used to coat a given substrate at a prescribed production rate. The concept of the Coating windows was first developed for slot coating flow. Coating windows can be constructed either from extensive experimentation or from theoretical model.

Ruschak (1976) analyzed the coating window of a slot coating bead dominated by surface tension force (capillary pressure) in the upstream and downstream menisci; Silliman (1979) and Higgins and Scriven (1980) took the viscous drag of the substrate and die lips into account. More advanced theoretical analyses and experiments on the limits of operability and flow stability within those limits were made subsequently (Sartor (1990), Gates and Scriven (1996), Carvalho and Kheshgi (2000), Romero et al. (2004)). A sketch of the operability limit is presented in Fig. 2. The figure shows that the coating window is bounded by three modes of failure:

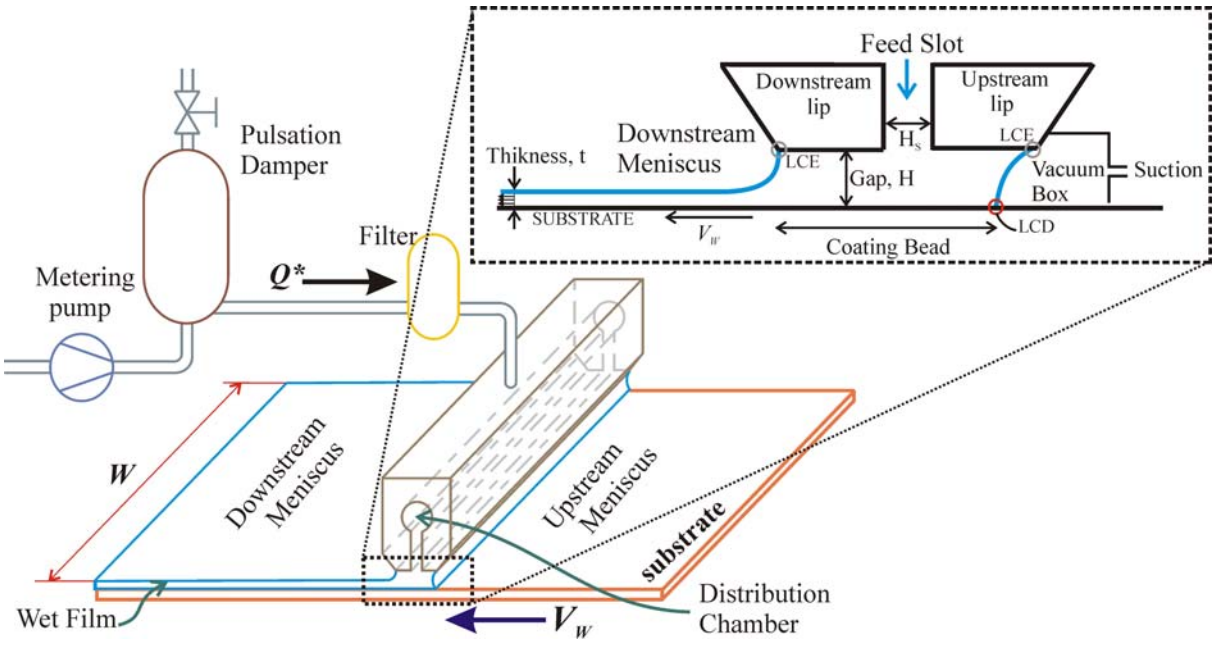


Figure 1. Sketch of the basic elements of Slot Coating and detail of the coating bead with the die lip.

1. When the coated layer is thicker than the thinnest that can be produced at a fixed gap and substrate speed, i.e. $t > t_{\min}$ in Fig. 2, too great a vacuum at the upstream free surface causes liquid to be drawn along the die surface into the vacuum chamber. This diversion of liquid destroys pre-metering.
2. Too little vacuum at the upstream free surface leaves the net viscous drag force on the upstream part of the bead unbalanced by the pressure gradient that is imposed by capillary pressure forces in the menisci upstream and downstream and the difference in external pressure on those menisci (i.e. vacuum). In consequence the upstream meniscus shifts toward the feed slot until the bead drastically rearranges into a three-dimensional form that delivers separate rivulets to the substrate. Between the rivulets are dry lanes that extend upstream through the bead. Along those lanes air is sucked into the vacuum chamber. It is in this regime that, at given vacuum (ambient pressure downstream minus air pressure exerted on upstream meniscus), there is a lower limit to the thickness of continuous liquid layer that can be coated from a downstream gap of specified clearance. As Fig. 2 shows, the limit can be lowered by applying greater vacuum and thereby shifting the upstream meniscus away from the edge of the feed slot.
3. At given substrate speed, too low a flow rate per unit width from the slot causes the downstream meniscus to curve so much that it cannot bridge the gap's clearance $H$. Consequently the meniscus becomes progressively more three-dimensional, alternate parts of it invading the gap until the bead takes a form that delivers separate rivulets or chains of droplets to the substrate moving past. This transition from a continuous coated liquid layer is what is called here the low-flow limit: the minimum thickness of liquid that can be deposited from a gap of specified clearance at a given substrate speed. And, as Fig. 2 makes plain, it is independent of the vacuum applied, given that the vacuum is great enough to draw the upstream meniscus away from the feed slot. The outcome is the same when at a given flow rate per unit width from the slot; the substrate speed is too high. In this case, the low-flow limit is sometimes referred to as the high-speed limit (see Carvalho and Kheshgi (2000)). The outcome is essentially the same when at a given flow rate per unit width from the slot and a given substrate speed, the clearance of the downstream gap is too great. In this case, the low-flow limit is referred to as the wide-gap limit: the maximum gap from which a given thickness of liquid coating can be deposited on a substrate moving at specified speed.

The center piece in slot coating process is the coating die. Many different die designs are show in the patent literature, publications and brochures form die manufacturers. The external design, in particular the shape and the positioning of the coating die relative to the substrate, is varied to find an ideal design for any application. Fig. 3 show different geometries of the coating die. The lip geometry influences the liquid flow and the pressure distribution in the coating gap (see Kistler and Schweizer (1997)) leading to different flow configurations.

Gates (1999) was able to complete a comprehensive array of flow visualizations of single layer slot coating. In each case the liquid was Newtonian, but a slot die featured interchangeable lips enabled him to make experimental observations about the effects of die lip geometry. The experimental analysis was complemented with a viscocapillary model. Figures 3e), 3f) and 3g) show the die lip shapes that Gates used in his flow visualizations.

The visco-capillary model is only valid at low capillary numbers, i.e., typically low speed and/or low viscosity. However, many coating process do not operate at low capillary numbers, especially those at high web speeds.

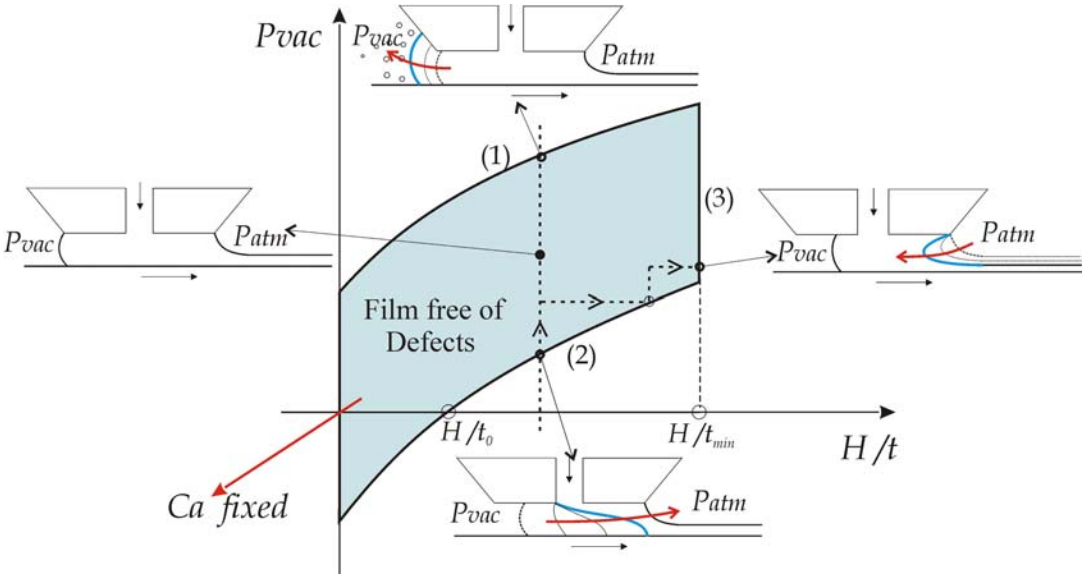


Figure 2. Coating Windows of a slot coating process, in the plane of vacuum *Pvac* vs gap-to-thickness ratio $H/t$, at a fixed capillary number *Ca*. The boundaries of the window are set by different bead break-up mechanisms. *tmin* represents the minimum film thickness that can be deposited onto the substrate at a given capillary number.

In this work, the coating window at different operating conditions, including high capillary number, was determined by theory, using a theoretical approach that consisted of solving the two dimensional Navier-Stokes equations with free surface that describe liquid flow in the coating bead by the Galerking/finite element method. A Pseudo-arc-length continuation was used to construct a solution path as the flow rate fed into the die was diminished. The minimum film thickness corresponded to the flow rate at which a turning point on the solution path occurred.

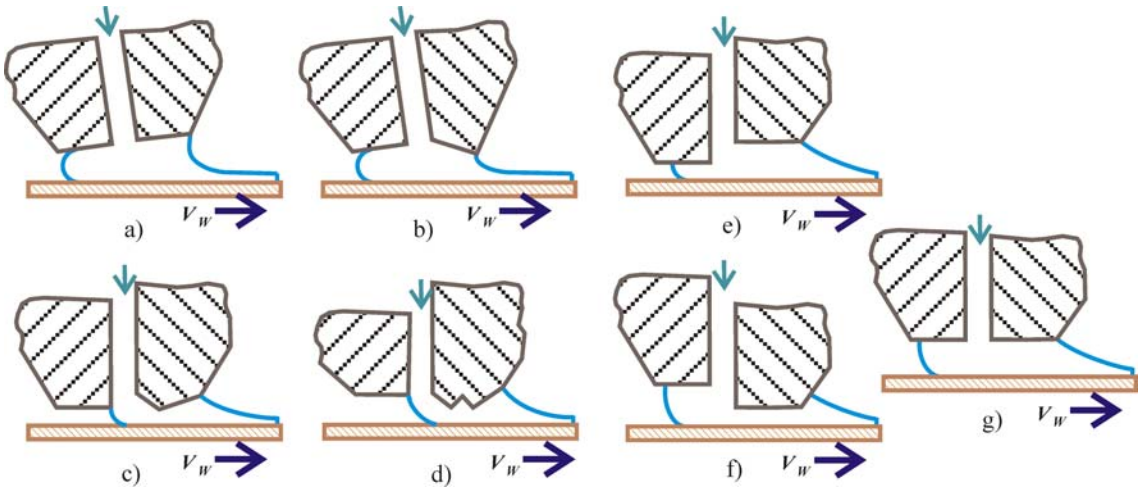


Figure 3. Die design of Slot coater: a) Divergent die lip; b) Convergent die lip; c) Convergent/divergent die lip; d) Two convergent /divergent die lip; e) Underbite lip; f) Overbite lip, g) Uniform or Standard lip.

**2. Theoretical model and solution method**

The flow in the coating bead is strongly affected by following operating parameters: gap (*H*), flow rate (*Q=Q*/W*), web speed ($V_w$), die configuration and liquids and roll cover properties.

### 2.1. Equation of the liquid flow

Figure 4 shows the liquid domain, bounded by two liquid-air interfaces, the coating die surface and the substrate. Coating flows are laminar, and ideally at steady-state and two-dimensional. The motion of the liquid is described by the momentum equation and continuity equation of incompressible flow:

$$\rho \mathbf{v} \cdot \nabla \mathbf{v} = \nabla \cdot \mathbf{T} \tag{1}$$

$$\nabla \cdot \mathbf{v} = 0 \tag{2}$$

For Newtonian liquid, the stress tensor **T** is given by:

$$\mathbf{T} = \left[ - p\mathbf{I} + \mu(\nabla \mathbf{v} + \nabla \mathbf{v}^T) \right] \tag{3}$$

$\rho$ and $\mu$ are the density and viscosity of the flowing liquid, e **v** the velocity vector.

### 2.2. Boundary condition

The boundary conditions for theoretical modeling in slot coating are also shown in the Fig. 4.

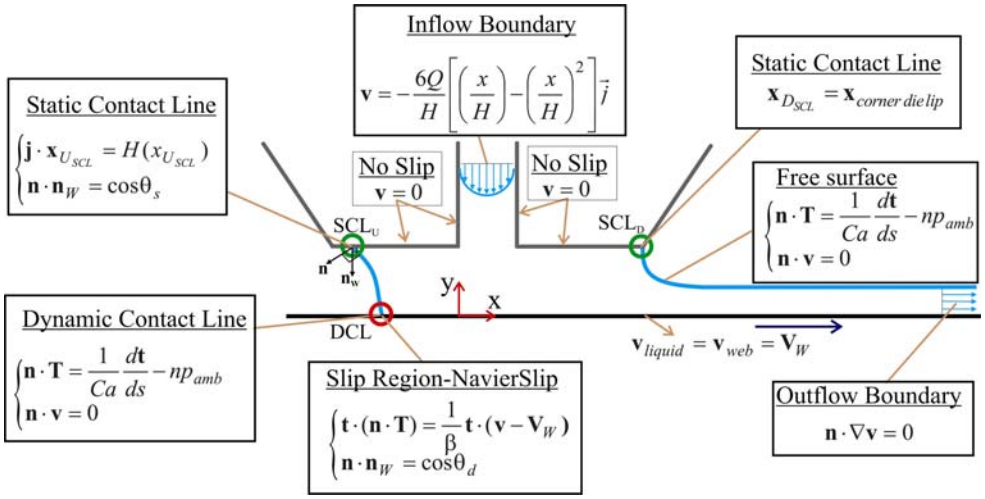


Figure 4. Sketch of the slot coating with boundary conditions for theoretical modeling

The relevant dimensionless parameters are:

- The Capillary number: $Ca = \frac{\mu V_W}{\sigma}$;
- Reynolds number: $\mathrm{Re} = \frac{\rho V_W H}{\mu}$;
- Dimensionless Slot Height: $\frac{H_S}{H}$.
- Vacuum pressure: $Vac = \frac{P_{vac} H}{\sigma}$;
- Gap to thickness ratio: $\frac{H}{t}$;

The governing equations give rise to a free boundary problem, because the positions of the gas-liquid interfaces are unknown a priori. The solution of such problems is recounted briefly here. Fuller accounts were given by Kistler and Scriven (1984), Sackinger, Schunk, and Rao (1996) and Carvalho and Scriven (1997).

### 2.2. Mapping from the physical to reference domain

In order to solve a free-boundary problem using the standard techniques of boundary value problem, the set of differential equations posed in the unknown physical domain $\Omega$ has to be transformed to an equivalent set defined in a suitable known reference domain $\overline{\Omega}$, as sketched in Fig. 5. This is done by the mapping $\mathbf{x} = \mathbf{x}(\xi)$ that connects the two domains. Here, the unknown physical domain is parameterized by the position vector $\mathbf{x}$, and the reference domain by $\xi$. The reference domain adopted is to some extent arbitrary, with the conditions that the boundaries of the reference domain have to be continuously mapped onto the boundaries of the physical domain and the mapping has to be invertible.

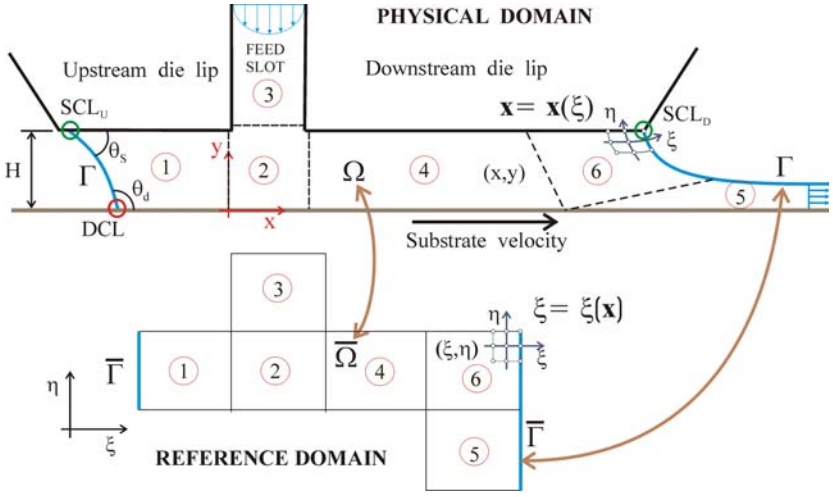


Figure 5. Sketch of mapping from the liquid domain to the reference domain

The mapping used here is presented in detail by de De Santos (1991). He showed that a functional of weighted smoothness can be used successfully to construct the sorts of maps involved here. The inverse of the mapping that minimizes the functional is governed by a pair of elliptic differential equations identical to those encountered in diffusion transport with variable diffusion coefficients. The coordinates $\xi$ and $\eta$ of the reference domain satisfy:

$$\nabla \cdot D_\xi \nabla \xi = 0 \; ; \quad \nabla \cdot D_\eta \nabla \eta = 0 \tag{4}$$

The coefficients, $D_\xi$ and $D_\eta$, are controlled by stretching functions along iso-$\xi$ and iso-$\eta$ coordinates lines (Benjamin et al 1990)

Boundary conditions are needed to solve the second-order partial differential equations. Along solid walls and synthetic inlet and outlet plates, the boundaries are located by imposing a relation between the coordinates and from the equation that describes the shape of the boundary and stretching functions are used to distribute the points along the boundaries. The free boundary (gas-liquid interface) is located by imposing the kinematic condition. The discrete version of the mapping equations are generally referred to as mesh generation equations. Spatial derivatives with respect to coordinates of the physical domain x and y can be written in terms of derivatives with respect to the coordinates of the reference domain $\xi$ and $\eta$ by using the inverse of the gradient of the mapping:

$$\nabla_x \phi = \mathbf{J_T}^{-1} \nabla_\xi \phi \tag{5}$$

Where $\mathbf{J_T}$ is the Jacobian of the transformation

### 2.3. Finite element formulation of the system equations

The system of partial differential equations presented in the previous section is solved by Galerkin's/Finite Element method. The velocity and node position are represented in terms of bi-quadratic basis functions $\phi_j$ and the pressure with linear discontinuous functions $\chi_j$:

$$\mathbf{v} = \sum_{j=1}^{9} (\mathbf{v}_j \phi_j) \; ; \quad \mathbf{p} = \sum_{j=1}^{3} (P_j \chi_j) \; ; \quad \mathbf{x} = \sum_{j=1}^{9} (\mathbf{x}_j \phi_j) \tag{6}$$

The Galerkin weighted residual of the continuity, momentum and mesh generation (mapping) are given by:

$$\mathbf{R}_c^i = \int_{\overline{\Omega}} (\nabla \cdot \mathbf{v}) \chi_i J_T d\overline{\Omega}, \tag{7}$$

$$\mathbf{R}m_x^i = \int_{\overline{\Omega}} \left[ \rho\phi_i \left( u\frac{\partial u}{\partial x} + v\frac{\partial u}{\partial y} \right) + \left( \frac{\partial \phi_i}{\partial x} Txx + \frac{\partial \phi_i}{\partial y} Txy \right) \right] J_T d\overline{\Omega} - \int_{\overline{\Gamma}} \phi_i (\mathbf{n} \cdot \mathbf{T})_x \left(\frac{d\Gamma}{d\overline{\Gamma}}\right) d\overline{\Gamma} \tag{8}$$

$$\mathbf{R}m_y^i = \int_{\overline{\Omega}} \left[ \rho\phi_i \left( u\frac{\partial v}{\partial x} + v\frac{\partial v}{\partial y} \right) + \left( \frac{\partial \phi_i}{\partial x} Txy + \frac{\partial \phi_i}{\partial y} Tyy \right) \right] J_T d\overline{\Omega} - \int_{\overline{\Gamma}} \phi_i (\mathbf{n} \cdot \mathbf{T})_y \left(\frac{d\Gamma}{d\overline{\Gamma}}\right) d\overline{\Gamma} \tag{9}$$

$$\mathbf{R}x^i = -\int_{\overline{\Omega}} D_\xi \left(\frac{\partial y}{\partial \eta}\frac{\partial \phi_i}{\partial x} - \frac{\partial x}{\partial \eta}\frac{\partial \phi_i}{\partial y}\right) d\overline{\Omega} + \int_{\overline{\Gamma}} D_\xi \frac{1}{J_T} \left(\frac{\partial y}{\partial \eta}\eta_x - \frac{\partial x}{\partial \eta}\eta_y\right) \phi_i \left(\frac{d\Gamma}{d\overline{\Gamma}}\right) d\overline{\Gamma} \tag{10}$$

$$\mathbf{R}y^i = -\int_{\overline{\Omega}} D_\eta \left(\frac{\partial y}{\partial \xi}\frac{\partial \phi i}{\partial x} - \frac{\partial x}{\partial \xi}\frac{\partial \phi i}{\partial y}\right) d\overline{\Omega} + \int_{\overline{\Gamma}} D_\eta \frac{1}{J_T} \left(-\frac{\partial y}{\partial \xi}\eta_x + \frac{\partial x}{\partial \xi}\eta_y\right) \phi_i \left(\frac{d\Gamma}{d\overline{\Gamma}}\right) d\overline{\Gamma} \tag{11}$$

Where $J_T$ is the determinant of Jacobean of the transformation.

The system of partial differential equations reduces to simultaneous algebraic equations for the coefficients of the basis functions of all the fields. This set of equations is non-linear and sparse. It was solved by Newton's method, which requires evaluation of the full jacobian matrix.

$$\mathbf{c}^{(k+1)} = \mathbf{c}^{(k)} + \delta\mathbf{c}; \quad \mathbf{J}(\delta\mathbf{c}) = -\mathbf{R}; \quad \mathbf{J}_{ij} = \frac{\partial \mathbf{R}_i}{\partial \mathbf{c}_j} \tag{12}$$

Where $\mathbf{c}$ is the vector of the unknowns coefficient of the basis functions for the velocity, pressure and nodal positions, $\mathbf{R}$ is the vector of weighted residuals given by above equations.

The iteration proceeded until $\|\delta\mathbf{c}\|_2 + \|\delta\mathbf{R}\|_2 \le \varepsilon$. For each Newton's iteration, a linear system of equations was solved using **LU** decomposition. A pseudo-arc length continuation method coupled whit Newton's method it was used to automatically construct the entire path of steady state. The minimal film thickness at a given web speed was obtained by decreasing flow rate until a turning-point was found.

### 3. Results

In all the configurations considered here, i.e., overbite, underbite and standard lip configuration, the domain was divided into 474 elements, with approximately 10,000 unknowns. The representative geometries are shown in Fig. 6. The difference between them is the offset in the upstream die lip. The downstream gap $H_D = H = 100\,\mu\text{m}$ and the feed slot height $Hs/H = 0.75$ were kept constant. The Property number $P_P = \text{Re}/Ca = \rho\sigma H/\mu^2 = 2000$, that is a function of the liquid properties and coating gap and invariant to substrate speed, was also constant in all the cases.

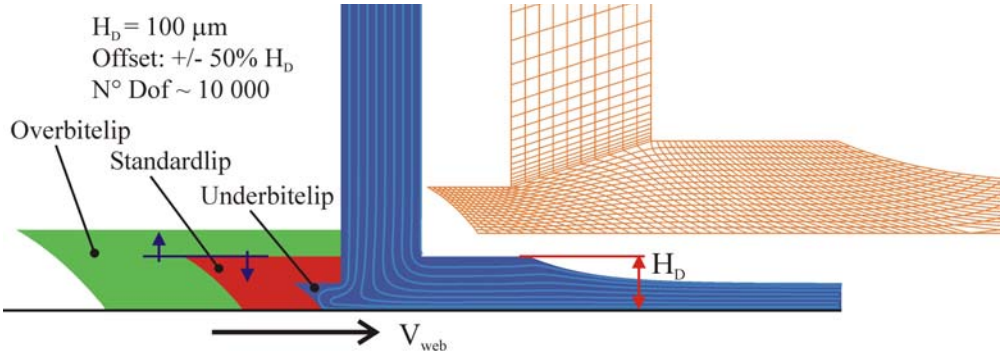


Figure 6. Sketches of the three die configuration used: Overbite, Standard and Underbite and the representative mesh of the Underbite type.

The limits on the operating condition were determined by following the solution path at a fixed web speed. The flow rate, and therefore the film thickness, was decreased until a turning point was encountered on the solution path. The critical gap-to-thickness ratio was calculated from the value of the flow rate at the turning point.

Figure 7 shows a path of solutions computed at different capillary number, Ca = 0.1; 0.5 and 1.0, at a vacuum pressure of Pvac = 14kPa, 80kPa and 160kPa, respectively. Flow states are characterized by the position of the dynamic contact line, $X_{DCL}$. This plot shows how the position of the dynamic contact line varies with the flow rate fed into the different die. As the coated film becomes thinner, the dynamic contact line is pulled towards the feeding slot. With the underbite configuration, the upstream meniscus was located closer to the feed slot and the position of the upstream meniscus was less sensitive to the film thickness. With the overbite configuration, the position of the upstream meniscus is more sensitive to the coated layer film thickness.

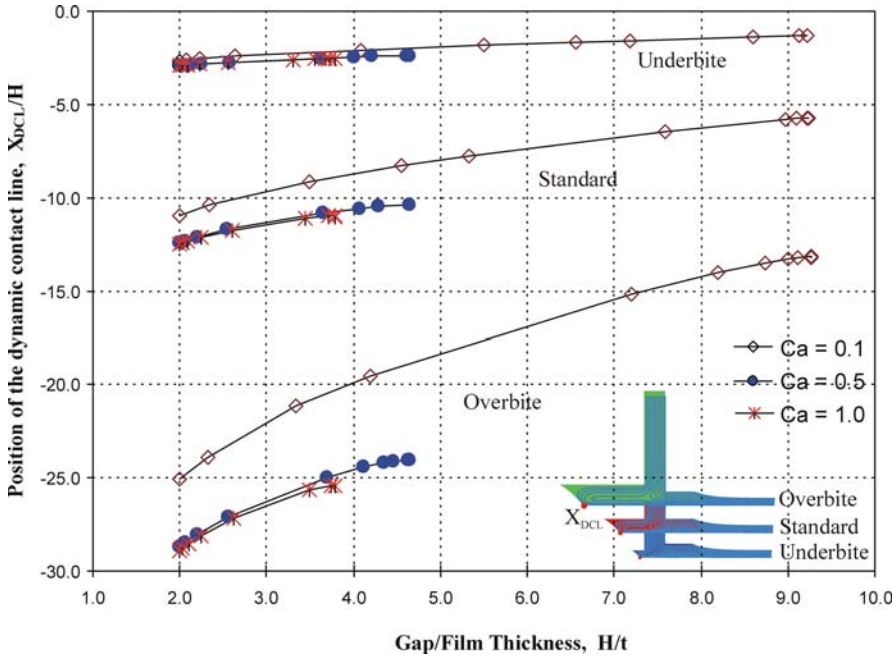


Figure 7. Position of the dynamic contact line as a function of the gap-to-thikcness ratio and capillary number.

Figure 8 shows the vacuum pressure necessary to maintain the process stable for the different upstream die lip configuration at *Ca = 0.1*. The Underbite configuration exhibit a larger range of vacuum operation than the other two configurations tested.

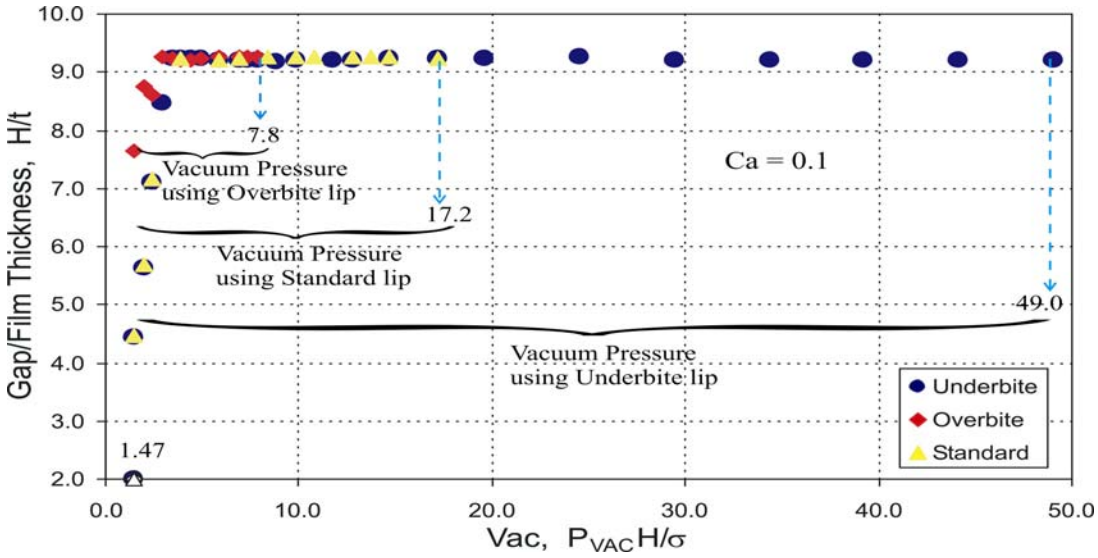


Figure 8. Range of vacuum pressure for different die configuration at *Ca = 0.1.*

The predicted coating window of slot coating process, in the plane of vacuum pressure and gap-to-thickness ratio at different capillary number and die lip configuration is shown in Fig.9. The upper boundary of the coating window is the upper vacuum limited. It was determined by raising the vacuum pressure until the upstream length of the coating bead became larger than the length of the upstream die lip. Beyond this value, the liquid would invade the vacuum box, leading to coating deffects. The lower boundary corresponds to the low vacuum limit. It was determined by decreasing the vacuum pressure until the upstream meniscus invades the region under the feed slot. In practice, the coating bead would break leading to rivulets. The left boundary of the coating window represents the minimum wet thickness that can be coated at a given substrate speed. The onset of this limit corresponds to the operating parameters at which the downstream free surface invades the coating bead. Experimental results indicated that meniscus becomes progressively more three-dimensional, alternate parts of it invading the gap until the bead takes a form that delivers separate rivulets or chains of droplets to the substrate moving past. In the theoretical model, this limit is represented by a turning point in the solution path. The minimum thickness is independent of the vacuum pressure applied, given that the vacuum is large enough to draw the upstream meniscus away from the feed slot.

The predicted coating window for the three geometries tested showed that the minimum thickness rises (gap-to-thickness falls) with capillary number, which means that thinner coating can only be obtained at low speeds. The effect of the die configuration in this process limit is very weak. The main effect of the die configuration is on the low and high vacuum limits. With the overbite coniguration, the pressure is the coating bead is higher because of the contraction in the gap, therefore the amount of vacuum needed to pull the upstream free surface is smaller.

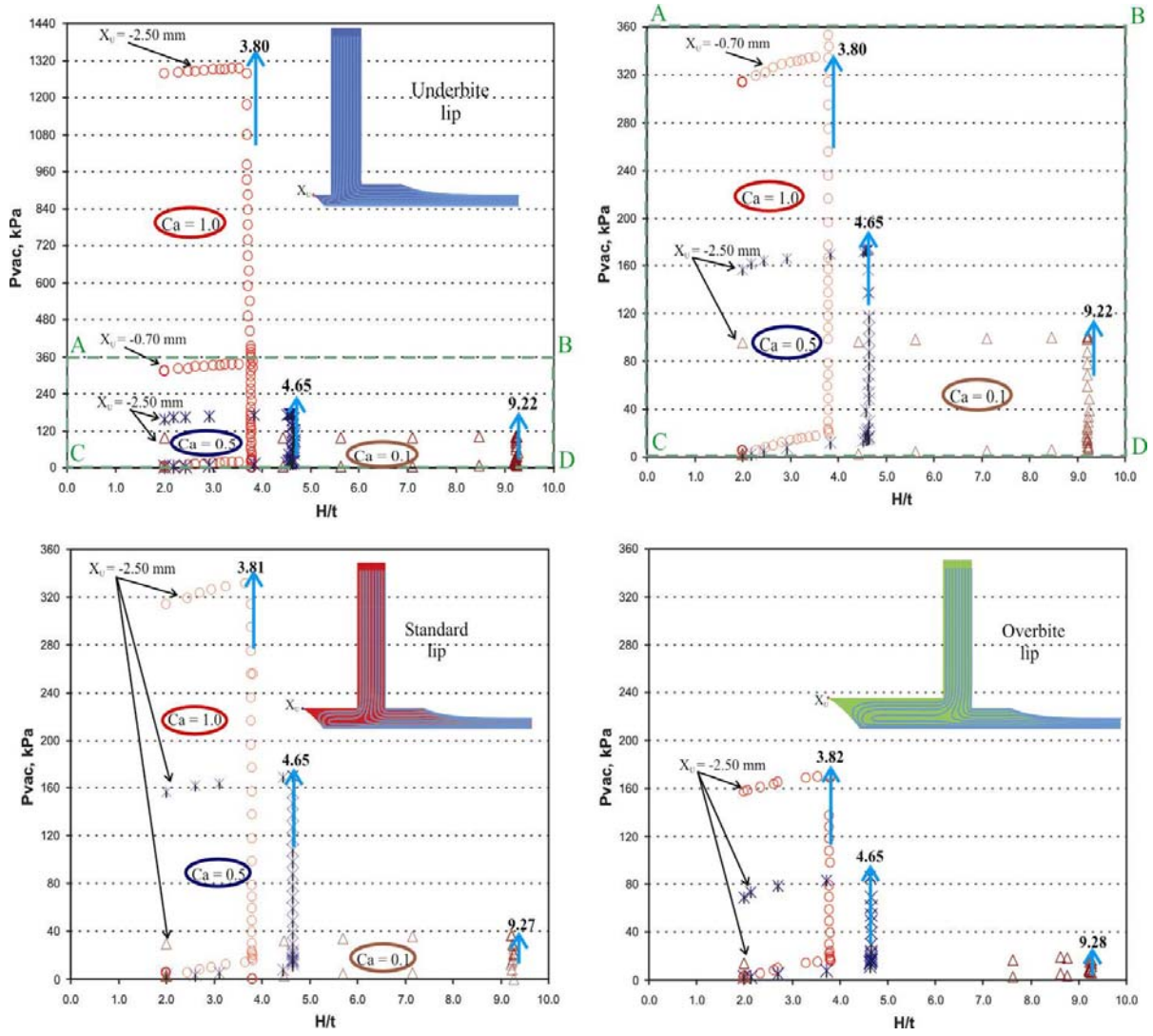


Figure 9. Coating Windows of a slot coating process, in the plane of vacuum *Pvac* vs gap-to-thickness ratio $H/t$ for different configuration of the die slot.

## 4. Final Remarks

The coating window of slot coating process was obtained theoretically by solving the two-dimensional Navier-Stokes equations with free surfaces. The results show how the die configuration affects the steady-state solutions and the limits of the important manufacturing process.

## 5. Referências

Beguin, A. L., 1954, "Method of Coating Strip Material", U.S.Pat.2,681,294

Benjamin, D. F., De Santos, J.M. and Scriven, L.E., 1990, "Meshs for viscous free surface flow as solutions to elliptic P.D.E.'s of transport.

Carvalho, M. S., and Scriven, L. E., 1997, "Flows in forward deformable roll coating gaps: Comparison between spring and plane strain models of roll cover". Journal of Computational Physics, 138(2), 449–479.

Carvalho, M. S. and Khesghi, H. S., 2000 "Low-Flow limit in slot coating: Theory and Experiments", AIChE Journal, 46, 1907-1917.

De Santos, J. M., 1991, "Two-phase cocurrent down flow through constricted passages". PhD Thesis, University of Minnesota, MN, USA.

Encit 2004, 2004, "Instruções para a Formatação de Trabalhos Submetidos ao 10º Congresso Brasileiro de Ciências Térmicas e Engenharia", ABCM, Curitiba, Brasil. 3 p.

Gates, I. D. and Scriven, L. E., 1996, "Stability Analysis of Slot Coating Flows", AIChE 1996 Spring National Meeting, New Orleans.

Gates, I.D., 1999, "Slot Coating flows: Feasibility, Quality", Ph. Thesis University of Minnesota. Published by University Microfilms International, Ann Arbor, MI.

Higgins, B. G. and Scriven, L. E., 1980, "Capillary pressure and viscous pressure drop set bounds on coating bead operatibility", Chemical Engineering Science, 35, 673-682.

Kistler, S. F., and Scriven, L. E., 1984. Coating flow theory by 8nite element and asymptotic analysis of the Navier–Stokes system. International Journal for Numerical Methods in Fluids, 4, 207.

Romero, O. J., 2003, Ph.D Thesis, University of PUC-Rio.

Ruschak, K. J., 1976 "Limiting Flow in a pre-metered coating device", Chemical Engineering Science, 31, pp 1057-1060.

Sackinger, P. A., Schunk, P. R., & Rao, R. R., 1996, "A Newton-Raphson pseudo-solid domain mapping technique for free and moving boundary problems, A Finite element implementation". Journal of Computational Physics.

Sartor, L., 1990, "Slot Coating: Fluid Mechanics and Die Design", Ph.D Thesis, University of Minnesota.

Silliman, W. J., 1979, "Viscous Film Flows with Contact Lines: Finite Element Simultions, A Basis for Stability Assessment and Design Optimization". PhD Thesis, University of Minnesota, MN.

## 6. Responsibility notice

The authors are the only responsible for the printed material included in this paper.